



ORIGINAL ARTICLE

Exploitation the unique acidity of novel cerium-tungstate catalysts in the preparation of indole derivatives under eco-friendly acid catalyzed Fischer indole reaction protocol



Hatem M. Altass^a, Moataz Morad^a, Abdelrahman S. Khder^{a,b,*}, Mohamed Raafat^c, Reem I. Alsantali^d, Menna A. Khder^b, Reda S. Salama^e, M. Shaheer Malik^a, Ziad Moussa^f, Mohammed A.S. Abourehab^g, Saleh A. Ahmed^{a,h,*}

^a Chemistry Department, Faculty of Applied Science, Umm Al-Qura University, 21955 Makkah, Saudi Arabia

^b Faculty of Science, Chemistry Department, Mansoura University, 35516 Mansoura, Egypt

^c Department of Pharmacology and Toxicology, College of Pharmacy, Umm Al-Qura University, Makkah 21955, Saudi Arabia

^d Department of Pharmaceutical Chemistry, College of Pharmacy, Taif University, P.O. Box 11099, Taif 21944, Saudi Arabia

^e Basic Science Department, Faculty of Engineering, Delta University for Science and Technology, Gamasa, Egypt

^f Department of Chemistry, College of Science, United Arab Emirates University, P.O. Box 15551, Al Ain, Abu Dhabi, United Arab Emirates

^g Department of Pharmaceutics, College of Pharmacy, Umm Al-Qura University, Makkah 21955, Saudi Arabia

^h Chemistry Department, Faculty of Science, Assiut University, 71516 Assiut, Egypt

Received 1 November 2021; accepted 22 December 2021

Available online 28 December 2021

KEYWORDS

Solid acid;
Cerium tungstate;
Catalyst;
Fischer indole reaction;
Eco-friendly protocol

Abstract Solid acidic cerium tungstate catalysts containing different molar ratios of cerium and tungstate were prepared by direct solvothermal methodology. The structure of the prepared catalysts was deeply studied and confirmed based on different characterization techniques such as DTA-TGA, FTIR, Raman spectra, XRD and N₂ adsorption measurements. Moreover, FTIR and TPD of chemically adsorbed pyridine techniques were conducted to fully address the nature and the strength of the acidic sites of the prepared catalysts. The study showed that at a lower molar ratio of tungstate, the catalyst contains cerium oxide phase and slight participation of cerium tungstate phase, which gradually increases with further increase of tungstate molar ratio. This phase change was also accompanied by a noticeable change in the thermal stability, surface area and

* Corresponding authors at: Chemistry Department, Faculty of Applied Science, Umm Al-Qura University, 21955 Makkah, Saudi Arabia.
E-mail addresses: askhder@uqu.edu.sa (A.S. Khder), saahmed@uqu.edu.sa (S.A. Ahmed).

Peer review under responsibility of King Saud University.



acidic properties of the prepared catalysts. Additionally, the techniques used to study the acidic properties showed an excellent enhancement in the acidic centers. It was also noted that the strength of these acidic centers reached the maximum in the case of using tungstate: cerium molar ratio 2:1 (CeW2.0) catalyst, and slightly decreased thereafter. By exploiting the acidic properties of the prepared catalysts, a series of indole derivatives were synthesized via the Fischer indole synthesis strategy. The results also showed that ~100% of indole derivatives were obtained using 0.02 g catalyst at 80 °C after 2 h only. Moreover, the Reuse experiment demonstrated the possibility of recycling and reusing the catalyst through many cycles with high efficiency, indicating its wonderful constancy and reusability.

© 2021 The Authors. Published by Elsevier B.V. on behalf of King Saud University. This is an open access article under the CC BY-NC-ND license (<http://creativecommons.org/licenses/by-nc-nd/4.0/>).

1. Introduction

The great development in industrial applications in the recent years leads to increased release of pollutants in the surrounding environment. These pollutants vary with different industrial processes, which have a very serious impact on the environment in addition to the high economic costs. That is why scientists have tended to use catalysts in industrial processes to reduce the harmful impact of these processes on the environment, as well as reduce economic costs (Fouad et al., 2011; Khder et al., 2016; Ahmed et al., 2008). In this regard, it became clear that the use of homogeneous catalysts such as mineral acids and others that have very harmful effects on the environment may sometimes seriously compromise or even outweigh the benefits of the industrial process itself. In addition, the use of homogeneous catalysis has a high economic cost due to the difficulty of separation and reuse. Therefore, the use of heterogeneous catalysis is considered the best solution to overcome these problems, whether environmental or economic, that accompany the use of homogeneous catalysis. Heterogeneous catalysts are characterized by ease of use, as well as ease of separation and reuse many times, which reduces the economic cost (Arata, 1996; Ahmed et al., 2013; Khder et al., 2008; Hassan et al., 2016; Ahmed et al., 2013). In this context, metal oxides are among the most widely used compounds because of their distinctive properties that can be developed and improved. One of the most important methods used to improve and develop these properties, especially acidic properties, is mixing (in different weight ratios) with other oxides, heteropoly acids, sulfate, phosphate, molybdate, tungstate, and others (Kulkarni et al., 2020; Ibrahim et al., 2021; El-Hakam et al., 1999; Khder and Ahmed, 2009; El-Hakam et al., 1999; Khder, 2008; Khder et al., 2016). In particular, cerium oxide is one of the rare earth oxide family that has attracted great attention for use in different environmental applications due to its tunable properties (Parwaiz et al., 2017; Geng et al., 2018; Altass et al., 2021). Moreover, modifying with tungstate species is one of the most important methods used to improve and modify the properties of cerium oxide, since tungstate are considered as a multifunctional class of oxide materials (Gupta et al., 2014; Pramanik and Bhattacharya, 2010; Khder et al., 2014). In the past, many attempts have been made to study the relationship between the surface tungstate species and the activity of the catalyst. The tungstate species may exist on the surface in many forms such as monotungstate, polytungstate, and crystalline WO_3 in which tungsten exhibits a tetrahedral or octahedral coordination environment (Inomata et al., 2015; Kishida and Watanabe, 2014; Abeyasinghe et al., 2017). Moreover, the strong acidity of the supported tungstate catalysts may be attributed to strong metal-tungsten interactions (Yong Kim et al., 2012; Kuba et al., 2003).

Indole derivatives rank among the most important families of organic heterocyclic compounds that have many applications in both industrial and pharmaceutical drugs (Roy et al., 2019; Abonia and Laali, 2019; Mkhwanazi et al., 2019; Zhou and Song, 2018). The significant applications of indoles motivated much research for the continuous discovery and development of new methodologies and strategies to

synthesize plenty of substituted indoles and discover their applications (Guo and Chen, 2018; Maurya et al., 2018; Ma et al., 2018). The Fischer indole synthesis (Fischer and Jourdan, 1883), discovered in 1883 by Emil Fischer, is a well-known beneficial organic reaction. In addition to the synthesis of indole rings, this versatile reaction is known to have extensive diversity applications in the total synthesis of bioactive natural products, bioactive molecules, and complexes (Chung et al., 2021; Jafarpour et al., 2020; Cui et al., 2020). In this reaction, the aromatic heterocycle indoles are synthesized from the reaction of phenylhydrazine derivatives with aldehydes or ketones under acidic homogenous catalysis strategies (Nazeri et al., 2020; Caiuby et al., 2020; Ahmed et al., 2019; Ahmed et al., 2004; Tomasulo et al., 2007). Generally, both Lewis and Brønsted acid catalysts were frequently used in this reaction, but these are hazardous and non-environmentally friendly (Org, 2007; Liu et al., 2017; Cai et al., 2017; Ruiz-Castillo and Buchwald, 2016).

In this work, cerium tungstate (CeW) catalysts with variable composition were prepared by the solvothermal method. The structure of the newly synthesized catalysts was confirmed based on different characterization techniques. The prepared catalysts were applied for the synthesis of some indole derivatives based on Fischer indole synthesis through a heterogeneous green approach. The approach features reaction conditions that follow an ecofriendly protocol. Moreover, the relationship between the catalyst composition, its acidity, and its catalytic activity have been studied.

2. Experimental

2.1. Materials

The chemicals used in the preparation of the catalyst were purchased from Sigma-Aldrich and those used in the synthesis of indole derivatives through the Fischer indole reaction (absolute ethanol, methyl isopropyl ketone, phenyl hydrazine, 4-methoxyphenyl hydrazine, 4-fluorophenyl hydrazine and 4-carboxyphenyl) were obtained from Merck.

2.2. Catalyst preparation

Cerium tungstate (CeW) catalysts with different cerium: tungstate molar ratios were prepared via direct precipitation method followed by a hydrothermal treatment route. In a typical procedure, two solutions of cerium nitrate hexahydrate and sodium tungstate each in 50 ml double deionized H_2O were separately prepared at room temperature. To precipitate cerium tungstate yellow gel, sodium tungstate solution was added slowly with vigorous stirring to cerium nitrate solution at room temperature for 3 h. The obtained gel was stirred for 24 h, transferred to a 100 ml stainless steel autoclave, then

heated to 160 °C for 20 h. Subsequently, the autoclave was cooled, the yellow gel was filtered, washed, and dried at 100 °C. Finally, the powder obtained was grained and calcined at 550 °C for 5 h. In this work, 5 samples of cerium tungstate (CeW) were prepared with cerium: tungstate molar ratios, starting from 1:0.5 in CeW0.5, to 1:2.5 in CeW2.5.

2.3. Catalyst characterization

The properties of the catalysts were studied by using many structural and textural tools. The thermograms (DTA and TGA) of dried samples were collected using a Shimadzu DTG-60 plus using α -Al₂O₃ as reference material. Prior to analysis, the samples were charged into Alumina pan and heated under N₂ atmosphere up to 800 °C. The FTIR spectra of some selected calcined samples were measured on a Shimadzu FTIR spectrophotometer. The crystal structure and phase identification were studied on Philips X'Pert diffractometer. The specific surface areas and pore structures of the calcined catalysts were further studied by nitrogen adsorption technique using QuantaChrome NOVA touch LX4 equipment at -196 °C. Prior to measurement, the catalysts were activated at 300 °C under vacuum. The structure and state of tungstate species were studied by analyzing Raman shifts using Thermo Scientific Raman spectrometer equipped with 532 nm laser as the excitation source at 8 mW power. The samples were also investigated using Scanning electron microscopy (SEM) (Quanta FEG 250, USA). The types and distribution of acid sites on the catalysts surface were characterized by using FTIR spectra of chemisorbed pyridine. The acid sites strength was also measured through pyridine TPD using Quantachrome Nova ChemBET equipment where the sample was heated to 800 °C in Ar atmosphere.

2.4. General procedures for the synthesis of substituted indoles via Fischer indole synthesis strategy

Firstly, two separate solutions of methyl isopropyl ketone (6 mmol) and substituted phenyl hydrazine (5 mmol) in ethanol were prepared. Then, the two solutions were carefully mixed in a 50 ml flask equipped with a condenser. Initially, the mixture was heated under reflux for 2 h to ensure complete dissolution of the reactants and prove that no product is formed in the absence of acidic conditions by monitoring the reaction with thin layer chromatography (TLC). Subsequently, 0.02 g of the CeW catalysts were carefully added. The heterogenous catalytic reaction was refluxed for the necessary reaction time and the progress of the reaction was monitored by TLC. At the end of the reaction, the catalyst was separated, and the ethanol was evaporated under reduced pressure. The products were spectroscopically pure, and no further purification was required. The chemical structures and purity of the indole derivatives were verified according to analytical and spectroscopic techniques. The obtained products were vacuum dried and the product yield percentages (%) were calculated according to equation (1):

$$\text{Yield (wt.\%)} = \frac{\text{actual weight of the product}}{\text{Theoretical weight of the product}} \times 100 \quad (1)$$

3. Results and discussion

3.1. Catalysts characterization

The thermal stability of the synthesized catalysts was studied by using the thermal analysis technique. The simultaneous Thermogravimetric-Differential thermograms (TGA-DTA) of some dried catalysts are presented in Fig. 1. All the catalysts exhibit a weight loss of about 11% between room temperature up to 250 °C on TGA curves (Fig. 1a), accompanied with endothermic effect on DTA curves (Fig. 1b) which may be attributed to the evaporation of physically and chemically adsorbed water molecules. Another small weight loss of about 2% is observed between 300 and 400 °C on TGA curves accompanied with a weak exothermic peak on DTA curves which can be ascribed to partial dehydroxylation of the catalyst surface (Koschker and Breit, 2016). Moreover, no other weight loss is observed on TGA curves above 400 °C of the samples, indicating that these samples are thermally stable. Another exothermic peak is observed at higher temperature at around 580 °C on DTA curves which may be attributed to the change of cerium oxidation state or change in phase since it is not accompanied by any weight loss on TGA curves (Yuzhakova et al., 2007; Maensiri et al., 2007). Moreover, the intensity of the higher temperature exothermic peak experiences a significant reduction and almost vanishes as the W: Ce ratio is increased, which may indicate the enhancement of cerium tungstate phase stability (*vide infra*). According to the thermal analysis results, 550 °C is selected for calcination of the prepared catalysts. The FTIR spectra of some selected catalysts are displayed in Fig. 2. The catalysts exhibited similar absorption FTIR bands between 400 and 1400 cm⁻¹, at about 450, 500, 730, 800, 835 and 930 cm⁻¹. The absorption bands at around 450, 500 and 800 cm⁻¹ are due to stretching vibrations of Ce—O bond (Venkatesh et al., 2016; Farahmandjou et al., 2016). Moreover, the samples also show other absorption bands at around 730, 833 and 930 cm⁻¹ attributable to different tungstate species. The absorption bands at around 730 and 835 cm⁻¹ may be assigned to stretching vibrations of W—O—W group (Thakur and Patil, 2014). Moreover, the absorption band at 930 cm⁻¹ is assigned to O—W—O symmetric stretching vibrations (Dirany et al., 2016; Liu et al., 2013). The absorption bands of both W—O—W and O—W—O stretching vibrations are characteristic of tetrahedral tungstate (WO₄²⁻) (Dirany et al., 2016). On the other hand, no FTIR absorption bands are observed due to the presence of a separate WO₃ phase on the surface even at a higher tungstate molar ratio. The X-ray diffraction technique was used to identify the crystal nature and the phase quality of the synthesized catalysts. The XRD patterns of all catalysts calcined at 550 °C are depicted in Fig. 3. As it can be seen, CeW0.5 sample exhibits a mixture of two different crystalline structures of cerium compounds. The first crystalline structure shows peaks identical with CeO₂ with cubic fluorite structure (JCPDS card no. 34-0394) (Liu et al., 2013). While the second crystalline structure diffraction peaks of CeW0.5 samples matched well with the monoclinic phase Ce₂(WO₄)₃ scheelite structure (JCPDS card no. 31-0340) (Kumar et al., 2017). Moreover, when Ce: W ratio changes from 1: 0.5 to 1:1 the main diffraction peak of CeO₂ phase at 2 θ = 28.5° is reduced, indicating a notable decrease in the percentage of CeO₂ phase compared to Ce₂(-

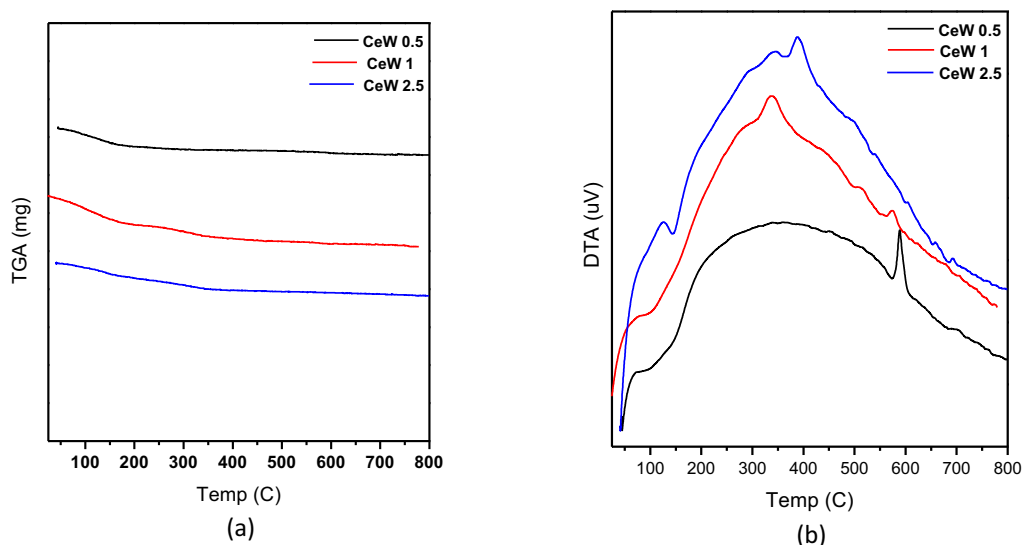


Fig. 1 (a) TGA thermograms, (b) DTA thermograms of some selected samples calcined at 550 °C.

WO_4)₃ phase. Further increase of Ce:W molar ratio to 1:1.5, 1:2 or 1:2.5 is accompanied by a complete disappearance of the CeO_2 phase, where only monoclinic $\text{Ce}_2(\text{WO}_4)_3$ phase is observed. The X-ray diffraction results show the effect of the Ce:W ratio on the phase formed in the catalysts calcined at 550 °C. Where a considerable ratio of CeO_2 has formed at a lower Ce:W molar ratio (1:0.5). Thereafter, the CeO_2 phase ratio decreases with the gradual increase of tungsten until it completely disappears when the Ce:W molar ratio reaches 1:1.5 and continues up to 1:2.5. These results are in excellent agreement with the thermal analysis, where the appearance of the sharp exothermic peak at 590 °C may be attributed to the change of oxidation state of the cerium in the CeO_2 phase (which contributes high ratio) in CeW0.5 sample (Yuzhakova et al., 2007; Maensiri et al., 2007). Additionally, the intensity of this exothermic peak decreases and is shifted to a lower tem-

perature (575 °C) when the Ce:W molar ratio becomes 1:1 where the ratio of CeO_2 decreases. Moreover, this high temperature exothermic peak disappears completely in CeW2.5 sample due to the absence of CeO_2 phase. The Raman spectra collected at room temperature of our samples calcined at 550 °C are shown in Fig. 4. The samples exhibited Raman spectra with different intensities distinctive for tungstate with the scheelite type structure (Thakur and Patil, 2014). The bands at 70 and 100 cm^{-1} are attributed to symmetric bending (B_g) and stretching (E_g) vibrations of O-Ce-O. The band observed at 192 and 381 cm^{-1} are attributed to free rotation (A_g mode) and symmetric bending (E_g) vibrations of $[\text{WO}_4]$ groups (Khder et al., 2016; Thakur and Patil, 2014). Another Raman bands are observed at around 278 and 329 cm^{-1} are ascribed to W-O-W bending mode (F_{2g}), while the bands at 726 and 810 cm^{-1} are assigned to W-O stretching (A_{1g}) and bending (E_g) modes respectively (Thakur and Patil, 2014; Khder et al., 2021; Mamede et al., 2004). The Raman bands observed at 920 and 940 cm^{-1} are due to symmetric stretching vibration (A_g mode) of W=O bonds in $\text{Ce}_2(\text{WO}_4)_3$ (Banares

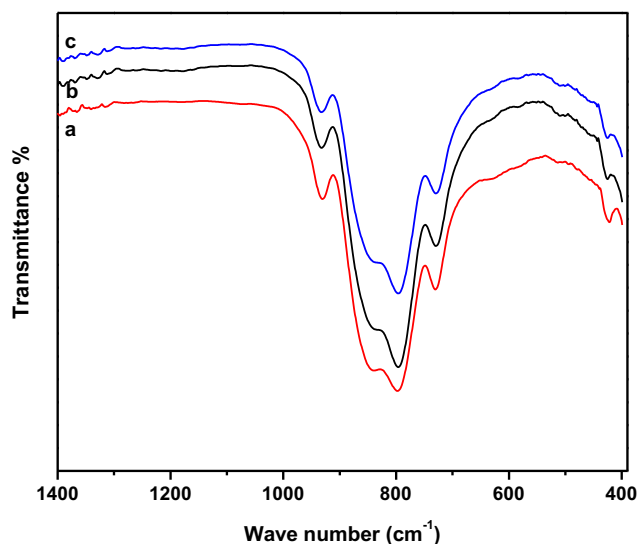


Fig. 2 FTIR spectra of: (a) CeW0.5, (b) CeW1.5 and (c) CeW2.5 samples calcined at 550 °C.

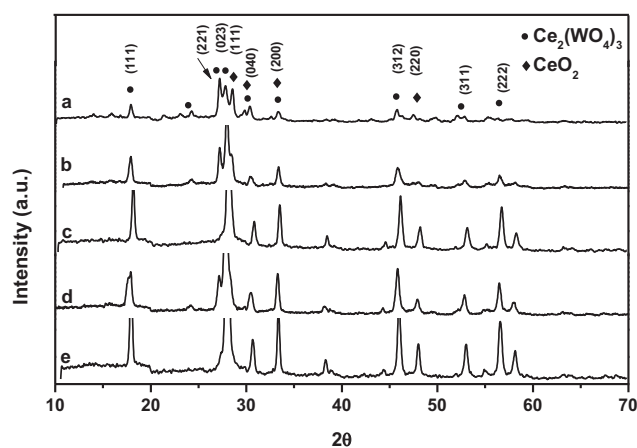


Fig. 3 X-ray diffraction patterns of: (a) CeW0.5, (b) CeW1, (c) CeW1.5, (d) CeW2 and (e) CeW2.5 samples calcined at 550 °C.

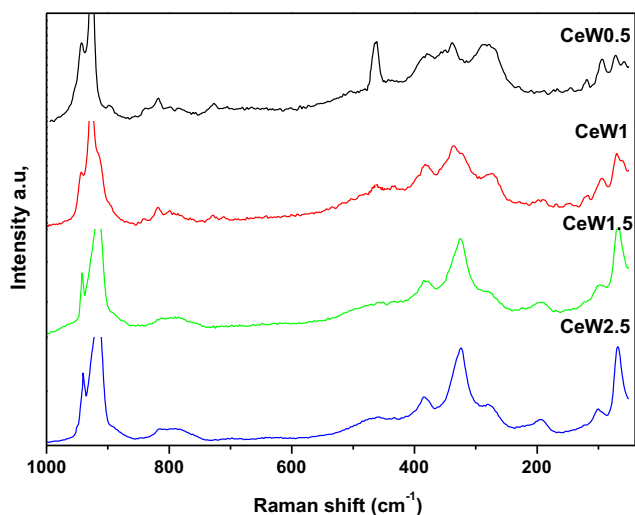


Fig. 4 Raman spectra of some selected samples calcined at 550 °C.

and Wachs, 2002; Bigey et al., 2001). The Raman spectra results of our samples are in good agreements with those previously reported in the literature (Mamede et al., 2004; Ross-Medgaarden and Wachs, 2007; Sugiura et al., 2016; Li et al., 2018). Moreover, the Raman spectra of CeW0.5 sample exhibited a band at 465 cm^{-1} which is ascribed to the symmetrical stretching vibration (F_{2g} mode) of (Ce—O), the typical band of cubic fluorite phase of CeO_2 (Luo et al., 2001). Additionally, the intensity of Raman band at 465 cm^{-1} is greatly decreased in CeW1 sample and nearly undetectable in the other samples. These results support the presence of mixture of cubic fluorite CeO_2 and $\text{Ce}_2(\text{WO}_4)_3$ scheelite structures in CeW0.5 sample and the percentage of CeO_2 is decreased in CeW1 and disappear in the other sample, which agree well with XRD results. Adsorption – desorption of N_2 gas at -196 °C experiment was carried out to study the textural parameters of the synthesized catalysts. Fig. 5a shows the adsorption- desorption isotherms of N_2 gas at -196 °C over the synthesized catalysts. The results show that all the catalysts exhibit typical type II adsorption isotherm with H3 hysteresis loop. The H3 hysteresis loop exhibited by the catalysts is attributed to the contribution of some mesopores in the catalysts surface (Sing et al., 1985; Altass and Khder, 2018; Altass and Khder, 2018; Al-Shehri et al., 2020). It was also found that the values of the textural properties change according to Ce:W molar ratio. As it is observed that the specific surface area (S_{BET}) and the total pore volume are increased steadily up to the maximum value at 79.9 m^2/g and 0.022 cc/g at Ce:W molar ratio of 1:1.5. Further increase of the Ce:W molar ratio to 1:2.5, is accompanied by a notable decrease in both surface area (S_{BET}) and pore volume (Table 1). The pore size distribution curves of all catalysts (Fig. 5b) show a narrow and uniformed peak in the range of 2.9–3.6 nm, which belongs to mesopores range (Al-Shehri et al., 2020). Moreover, the average particle radius (based on N_2 adsorption) is less than 100 nm which means that the samples are in the nanoscale. Additionally, results show that surface area of the samples increase with the initial increase of the mole ratio of Ce:W from 1:0.5 to 1:1.5, as the cerium oxide

phase gradually disappears (as shown by the XRD results), which means the combination of tungstate ions with cerium to form cerium tungstate. Moreover, when the molar ratio of Ce:W exceeds 1.5, then the excess of tungstate species may accumulate on the surface. The accumulation of tungstate species may lead to the notable decrease in the surface area (Shan et al., 2011). The morphology of CeW catalysts was characterized by using the SEM technique and the images are seen in Fig. 6. The CeW0.5 sample showed irregular spherical microstructure morphology with different diameters (Fig. 6a). Moreover, some changes in the morphology of the catalysts where some flower-like microstructures were clearly observed at higher tungstate ratios (Fig. 6b–e). These flower-like microstructures were built from two-dimensional sheet-like or plate-like structures. Many authors recently reported similar microstructure of many tungstate compounds (Lei and Bing, 2011; Cao et al., 2020).

The effect of Ce:W molar ratio on the acidic properties of the catalysts has been studied by using FTIR spectra of chemisorbed pyridine. Fig. 7a shows the collected FTIR spectra of all catalysts with different Ce:W molar ratios. The catalysts exhibit a mixture of Lewis and Brønsted acid sites represented by the FTIR bands at 1454 cm^{-1} for pyridine adsorbed at Lewis acid sites and at 1560 and 1650 cm^{-1} for pyridine adsorbed at Brønsted acid sites. Moreover, another peak is observed at 1490 cm^{-1} which is due to pyridine adsorbed on adjacent Lewis and /or Brønsted acid sites (Altass and Khder, 2016; Khder et al., 2018; Khder et al., 2012). The FTIR results of Chemisorbed pyridine demonstrate that, CeW0.5 sample exhibits limited contribution of Lewis and Brønsted acid sites. The results also showed, as shown in the figure, a remarkable enhancement in both types of acidic centers with the changes in the composition of the catalysts, reaching the maximum value in the CeW2 sample. The results of measuring the acidic properties of catalysts implies the effect of the molar ratio of Ce:W, which affects the state and distribution of a different tungstate species on the catalyst surface. Pyridine-TPD experiment is conducted to assess the acidity strength of the samples calcined at 550 °C. The collected Py-TPD profiles of some selected samples are presented in Fig. 7b. Three pyridine desorption peaks can be observed centered at around 130, 195 and 325 °C, indicating the coexistence of mixture of weak, moderate and strong acid sites respectively. The first and second peaks are overlapped, which indicates gradual change from poor to moderate acid sites, while the third peak is extended up to 600 °C. The results indicate that CeW0.5 sample exhibits lower acidity compared to other samples, with further increase in Ce:W ratio, notable enhancement of weak, moderate and strong acid sites is observed. The results also show that CeW2 contains a maximum amount of strong acid sites compared to weak and moderate types. This indicates that the increase of strong acidic centers occurs at the expense of weak and moderate acidic centers. On the other hand, the CeW2.5 sample exhibits higher amounts of weak and moderate acid sites compared to the strong type. The pyridine-TPD results confirms the higher contribution of strong acidic centers in CeW2 compared to other samples.

Based on previous studies, both unsaturated Ce^{4+} and W^{n+} ions are the main sources of Lewis type acidic centers. Whereas the acidic centers of Brønsted type, are generated on W—O—W, W=O and Ce—O—W sites supplied by cerium

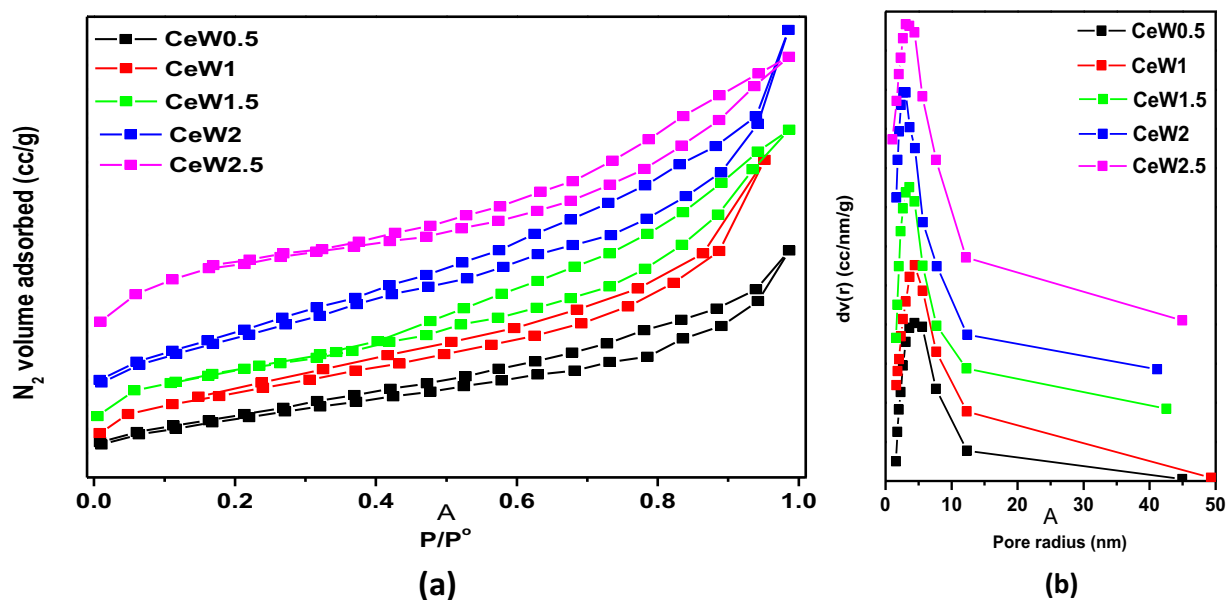


Fig. 5 (a) N_2 adsorption–desorption isotherms, (b) Pore volume distribution curves of all samples calcined at 550 °C.

tungstate ($Ce_2(WO_4)_3$) (Shan et al., 2012; Kobayashi and Miyoshi, 2007). This indicates the main and fundamental influence that tungstate plays in improving acidic centers of the Lewis and Brønsted type, which ultimately leads to a comprehensive augmentation of the acidic properties of the prepared catalysts. The results showed that increasing of the Ce:W molar ratio enhances the formation of the cerium tungstate phase. Meanwhile, as this increase is also accompanied by a noticeable increase in the surface area, thus leading to an improvement in the distribution of acidic centers on the surface, which ultimately leads to a significant improvement in the acid properties. By contrast, the discernible decrease in the surface acidity accompanying the further increase of Ce:W molar ratio may be attributed to the formation of amorphous tungstate (WO_x) that decrease the accessibility of pyridine to the acidic sites. Peng et al. proposed that the decrease in both Lewis and Brønsted acid sites at higher tungsten loading is attributed to the formation of isopolytungsten and WO_3 species on the catalyst surface (Peng et al., 2013).

3.2. Catalytic performance investigation

3.2.1. Synthesis of indole derivatives under heterogenous acid-catalyzed Fischer indole synthesis methodology

By exploiting the high acidic properties of the synthesized catalysts, an application to synthesize a series of interesting indole derivatives via the Fischer indole synthesis strategy under

green acid-catalyzed conditions have been successfully demonstrated as shown in Scheme 1. These synthesized indole derivatives are considered as key intermediates and important precursors for the synthesis of both photochromic spirobenzopyrans and spirooxazines.

As seen in Table 2, no evidence for the formation of any indole derivatives **3a-f** was detected when the reaction was carried out in the absence of the catalyst. It is worth mentioning that, on carrying the reaction in presence of 0.02 g of CeW2.0 using different substituted phenylhydrazines and isopropyl methyl ketone for 2 h, high yield (99.5%) and pure enough of indole derivatives were obtained (Table 2). On the other hand, the synthesized indole derivatives **3a-f** via acid catalyzed Fischer indole reaction were structurally confirmed by analytical and spectroscopic tools. For example, the IR-spectrum IR (ν cm^{-1}) of the 2,3,3-trimethyl-3H-indole-5-carboxylic acid (**3f**) showed the disappearance of $NHNH_2$ and $C=O$ of both starting materials and the following signals are shown up: a broad signal at 3455 cm^{-1} corresponding to the OH group, at 3049 , 3087 cm^{-1} for CH-aromatic, 2911 , 2926 cm^{-1} for CH-aliphatic and at 1699 for the carbonyl of the carboxylic acid group, 1605 cm^{-1} for $C=N$ and 1575 cm^{-1} for $C=C$ (Fig. S1). On the other hand, the 1H NMR (600 MHz, $CHCl_3$) (Fig. S2) of 5-methoxy-2,3,3-trimethyl-3H-indole (**3b**) showed the following signals: δ 1.28 (s, 6H), 2.23 (s, 3H), 3.81 (s, 3H), 6.80–6.81 (d, 1H, $J = 7.8$ Hz), 6.83 (s, 1H), 7.41–7.43 (d, 1H, $J = 8.4$ Hz); ^{13}C NMR (150 MHz, $CDCl_3$), (Fig. S3): δ

Table 1 Textural properties of different catalysts calcined at 550 °C.

Sample	S_{BET} (m^2/g)	Total Pore Volume (cc/g)	Average Pore radius (nm)	Average particle radius (nm)
CeW0.5	49.7	0.0145	2.99	95.75
CeW1	60.9	0.0181	3.33	75.23
CeW1.5	79.9	0.0220	3.57	60.54
CeW2	51.7	0.0180	3.06	93.79
CeW2.5	43.2	0.0139	3.61	97.70

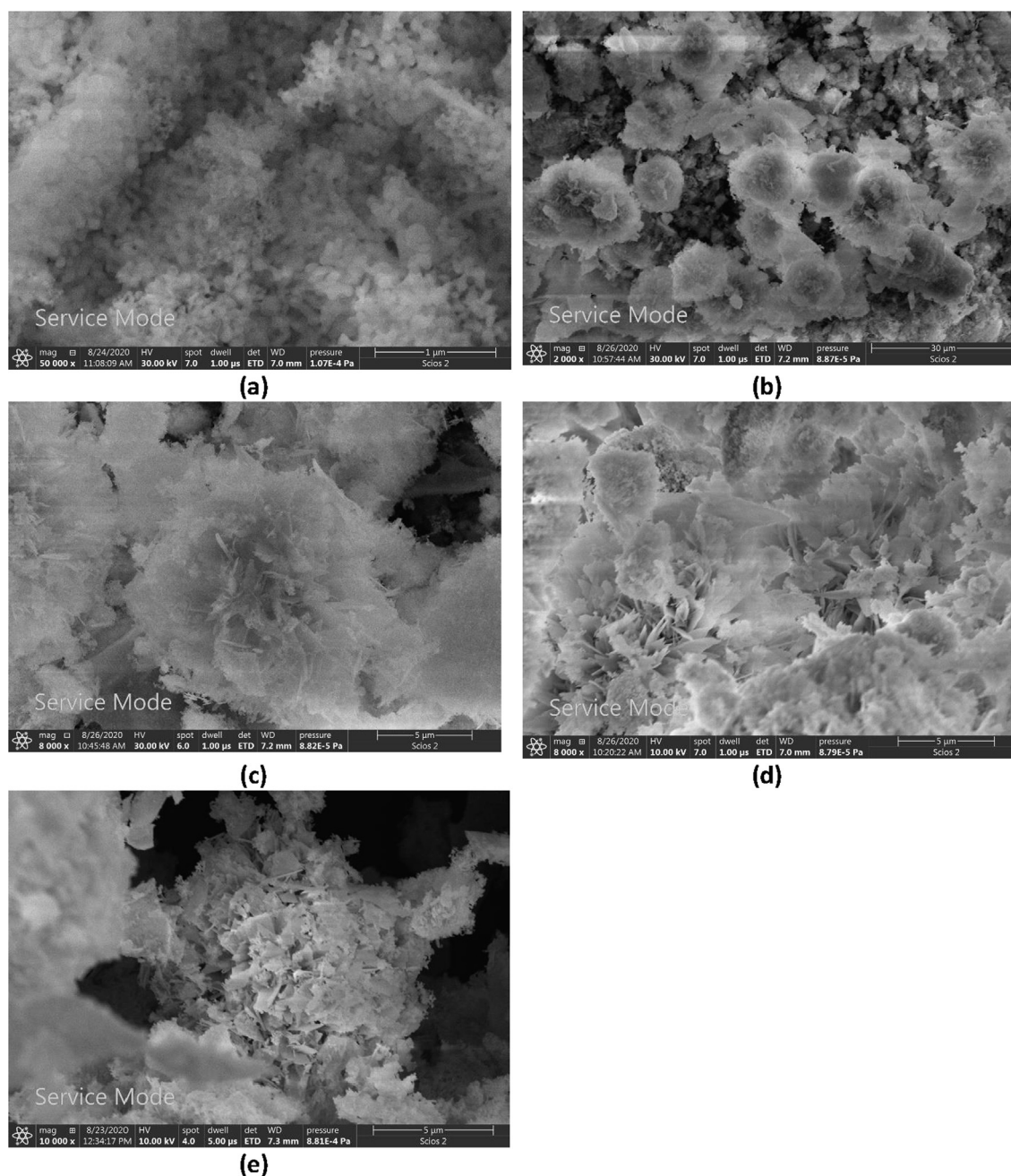


Fig. 6 SEM images of: (a) CeW0.5, (b) CeW1.0, (c) CeW1.5, (d) CeW2.0 and (e) CeW2.5 catalysts calcined at 550 °C.

15.22, 23.20, 53.74, 55.65, 108.13, 112.05, 120.02, 147.25, 147.27, 157.94, 185.28; Dept-135 NMR spectrum of 5-methoxy-2,3,3-trimethyl-3H-indole (**3b**) showed the complete disappearance of five quaternary carbons and only six signals are shown up (**Fig. S4**). Two signals at 15.22 and 23.19 for the methyl groups, one signal at 55.64 for methoxy group and three for CH-aromatic at 108.12, 112.04 and 120.01 ppm.

For optimization and demonstrating the significance of the acid catalysts in the Fischer indole synthesis, the reaction was performed to produce 2,3,3-trimethyl-3H-indole (**3a**) using 0.02 g of the catalyst under various reaction conditions. As seen in **Table 3**, at any reaction temperature, the % yield of 2,3,3-trimethyl-3H-indole (**3a**) gradually increases until it

reaches the maximum value in the case of CeW2.0 catalyst, and then slightly decreases thereafter. These results indicate strong acidic sites are required to catalyze the reaction. Additionally, to study the effect of reaction temperatures on the Fischer indole synthesis, the reaction was conducted over 0.02 g catalysts for 2 h at 25, 40, 60 and 80 °C. The results are listed in **Table 3**. Notably, low yield % of 2,3,3-trimethyl-3H-indole (**3a**) is observed at 25 °C, requiring substantial increase in the reaction temperature and reaction time as well. Moreover, significant increase of yield % of 2,3,3-trimethyl-3H-indole (**3a**) is observed when the reaction temperature is increased up to 80 °C, at which the highest yield is obtained. With further elevation in the reaction temperature,

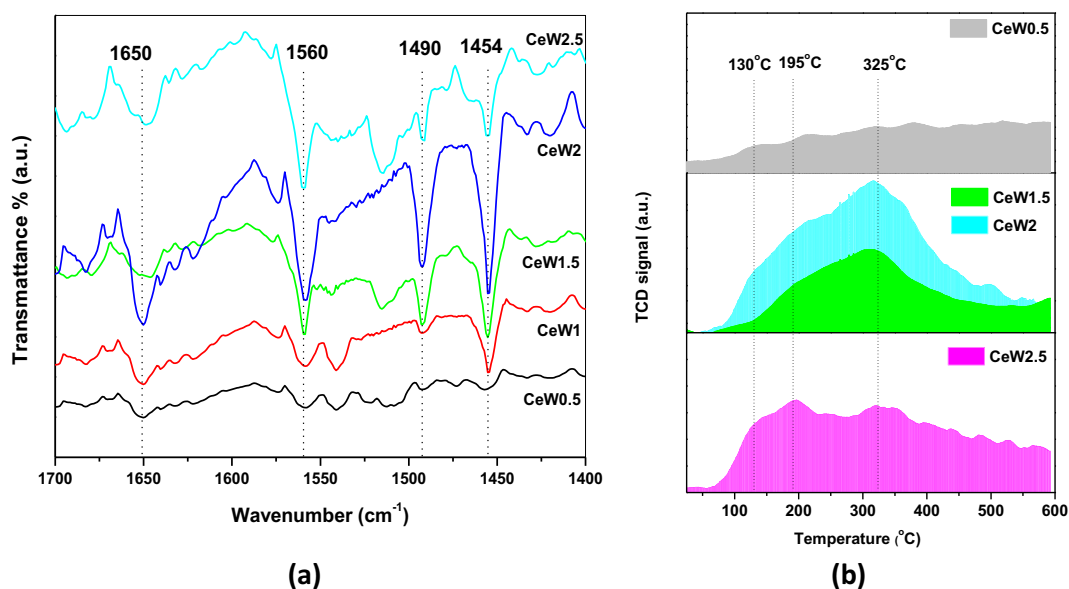
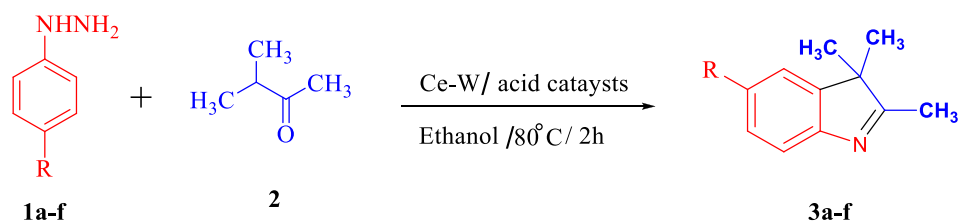


Fig. 7 (a) FTIR spectra of chemisorbed pyridine over samples calcined at 550 °C, (b) Pyridine-TPD profiles of CeW0.5, CeW1.5 and CeW2 samples.



Scheme 1 Acid-catalyzed Fischer indole reaction for the synthesis of indoles **3a-f** under CeW acidic heterogeneous catalysis strategy.

no notable increase in the yield % of indole derivatives was observed. Conversely, a decrease in the yield % occurs, which is probably due to product decomposition or some other side reactions, which are more favorable at high temperatures. Moreover, we also studied the influence of reaction time on the yield % of 5-methoxy-2,3,3-trimethyl-3H-indole (**3b**) over 0.02 g of CeW2.0 catalyst at 80 °C as shown in Fig. 8a. The obtained results reveal that the yield % of indole derivatives increase up to 99.5 % after 2 h, subsequently, less than 1%

increase of the yield % of indole derivatives is perceived after 2 h of the reaction, followed by no pronounced increase of the yield % until 5 h reaction time. These results indicate that 2 h was sufficient for the reaction to attain the equilibrium stage under the selected reaction conditions. For commercial and environment considerations we also studied the catalyst reusability. The study was carried out at 80 °C for 2 h over 0.02 g CeW2.0 catalyst and the results are presented in Fig. 8b. In this study, the catalyst was carefully isolated,

Table 2 Chemical structure and the yield % of the synthesized indole derivatives **3a-f** in ethanol over CeW2.0 catalyst at 80 °C for 2 h.

3	Chemical structure	Yield %	4	Chemical structure	Yield %
a		97.4	d		97.1
b		99.5	e		99.2
c		98.7	f		99.8

Table 3 Reaction condition optimization of the reaction condition for formation of 2,3,3-trimethyl-3H-indole (**3a**) via Fischer indole reaction under different Ce-W ratios in ethanol for 2 h at different temperatures.

Entry	Catalyst	Temp. (°C)	Time (h)	Yield (%)
1	No Catalyst	25–80	Up to 48	~0
2	CeW0.5	25	2	27.8
3	CeW0.5	40	2	54.5
4	CeW0.5	60	2	69.7
5	CeW0.5	80	2	87.4
6	CeW1.0	25	2	34.7
7	CeW1.0	40	2	49.3
8	CeW1.0	60	2	65.7
9	CeW1.0	80	2	90.2
10	CeW1.5	25	2	46.4
11	CeW1.5	40	2	58.7
12	CeW1.5	60	2	71.5
13	CeW1.5	80	2	93.4
14	CeW2.0	25	2	55.8
15	CeW2.0	40	2	73.9
16	CeW2.0	60	2	89.6
17	CeW2.0	80	2	99.5
18	CeW2.5	25	2	53.6
19	CeW2.5	40	2	67.4
20	CeW2.5	60	2	79.3
21	CeW2.5	80	2	97.8

washed three times with ethanol, and dried at 120 °C for 2 h. The obtained results prove that the catalyst can be reused 10 times successfully and without loss of its high efficiency and catalytic activity. Moreover, a notable enhancement in the yield % of obtained indole derivative by around 5% in presence of an electron-donating group substituted phenylhydrazine was observed. Frequently, the Fischer indole reaction cyclization reaction is a typical archetypal of acid catalyzed reaction (Bilal et al., 2021; Devkota et al., 2021). The positive and valuable results obtained in this investigation reveal the forthright relationship between the catalyst acidic properties and its employment in the clean synthesis of indole derivatives.

Furthermore, the results explain the imperative effect of Brønsted acidic centers on the catalytic competence of the reaction under exploration.

A typical and postulated mechanism of the Fischer indole reaction under heterogeneous acid catalysis protocol (Scheme 2) commences with exploiting the acidic properties of our synthesized acid catalysts. As such, they permit the reaction to proceed efficiently following the initial reaction of substituted phenylhydrazines and isopropyl methyl ketone to form phenylhydrazone which undergoes protonation by the acidic centers supplied by the acid catalysts and isomerizes to the corresponding enamine. Then, the protonated enamine undergoes

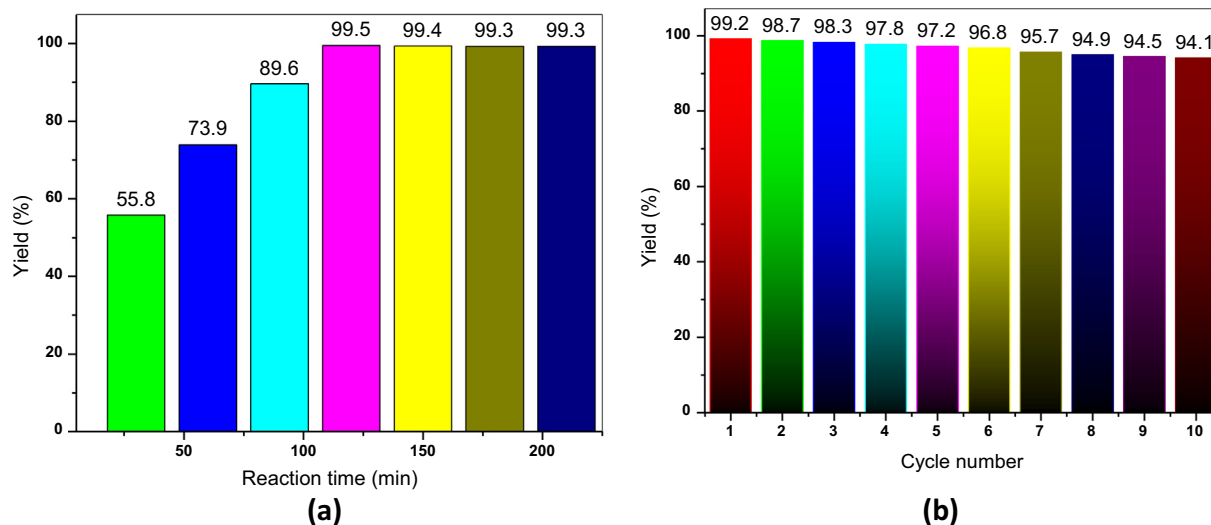
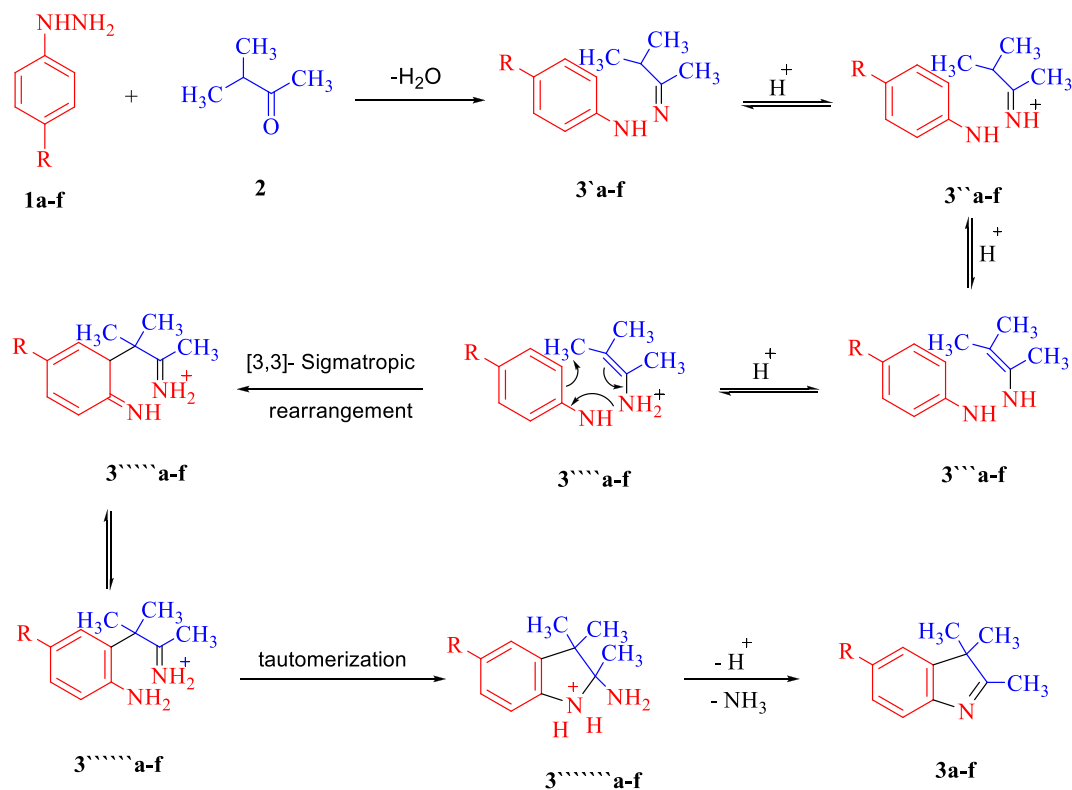


Fig. 8 (a) Effect of reaction time on the 5-methoxy-2,3,3-trimethyl-3H-indole (**3b**) over 0.02 g of CeW2.0 catalyst at 80 °C. (b) Reusability study over 0.02 g of CeW2.0 catalyst for the synthesis of 5-carboxy-2,3,3-trimethyl-3H-indole (**3f**) at 80 °C for 2 h.



Scheme 2 Postulated mechanism of Fischer indole reaction for the formation of 2,3,3-trimethyl-3H-indole derivatives (**3a-f**) under heterogeneous acid catalyzed approach.

an electrocyclic (Ahmed et al., 2008; Ahmed et al., 2008)-sigmatropic rearrangement in which the N-N bond is broken and imines are produced. A re-aromatization of the benzene ring of the formed double imine to stipulate an anilino imine, in which the imine undergoes intramolecular nucleophilic attack by the amino group to yield the amino indolines. The resulting imine forms a cyclic aminoacetal, which under acid catalysis, eliminates molecular NH_3 , resulting in the formation of indole derivatives **3a-f** under clean and eco-friendly heterogeneous catalysis.

4. Conclusion

In summary, cerium tungstate acid catalysts have been synthesized via a direct precipitation method followed by a hydrothermal treatment route. The catalysts were fully characterized using different techniques. The results showed that the molar ratios of tungstate and cerium are the main and important factor in determining the surface and textural properties of the prepared catalysts. It also showed that the types of acid centers and their strength change significantly with the change of these molar ratios. Additionally, both the number and strength of acidic centers reached their maximum when using twice the molar ratio of tungstate, as is evident in the CeW2.0 sample. It is worth mentioning that all the prepared catalysts displayed extraordinary prospects for applications in unique, eminent, and popular acid-catalyzed cyclization reactions such as Fischer indole synthesis, where indole derivatives were synthesized in high yields under clean, eco-friendly conditions. Optimization of the reaction conditions revealed that more than 99 % indole derivatives yields were successfully obtained when using 0.02 g of CeW2.0 at 80 °C for 2 h reaction time. Interestingly, the prepared acidic catalysts showed high recyclability and can be reused for many reaction cycles without a significant decrease in their catalytic efficacy. The obtained results suggest that the prepared acidic catalysts

will find new opportunities for further exploration in other related acid-catalyzed organic reactions at both laboratory and industrial-scale level.

Declaration of Competing Interest

The authors declare that they have no known competing financial interests or personal relationships that could have appeared to influence the work reported in this paper.

Acknowledgements

The authors would like to thank the Deanship of Scientific Research at Umm Al-Qurra University for supporting this work by Grant code (19-MED-1-01-0050). The authors would like to extend their sincere appreciation to Taif University Researchers Supporting Project number (TURSP-2020/312), Taif University, Taif, Saudi Arabia. Dr. Ziad Moussa is grateful to the United Arab Emirates University (UAEU) of Al-Ain and to the Research Office for supporting the research developed in his laboratory (Grant no. G00003291).

Appendix A. Supplementary material

Supplementary data to this article can be found online at <https://doi.org/10.1016/j.arabjc.2021.103670>.

References

Abeysinghe, D., Smith, M.D., Yeon, J., Tran, T.T., Sena, R.P., Hadermann, J., Halasyamani, P.S., Loye, H.-C., 2017. Crystal

- growth and structure analysis of $Ce_{18}W_{10}O_{57}$: a complex oxide containing tungsten in an unusual trigonal prismatic coordination environment. *Inorg. Chem.* 56 (5), 2566–2575.
- Abonia, R., Laali, K.K., 2019. Ionic liquid-mediated synthesis and functionalization of heterocyclic compounds. *Adv. Heterocycl. Chem.* 128, 333–431.
- Ahmed, S.A., Awad, M.I., Althagafi, I.I., Altass, H.M., Morad, M., Alharbi, A., Obaid, R.J., 2019. *J. Mol. Liq.* 291, 111356.
- Ahmed, A.I., El-Hakam, S.A., Samra, S.E., EL-Khouly, A.A., Khder, A.S., 2008. Structural characterization of sulfated zirconia and their catalytic activity in dehydration of ethanol. *Colloids Surf. A Physicochem. Eng. Asp.* 317, 62–70.
- Ahmed, A.I., El-Hakam, S.A., Khder, A.S., El-Yazeed, W.A., 2013. Nanostructure sulfated tin oxide as an efficient catalyst for the preparation of 7-hydroxy-4-methyl coumarin by Pechmann condensation reaction. *J. Mole. Catal. A: Chem.* 366, 99–108.
- Ahmed, A.I., Samra, S.E., El-Hakam, S.A., Khder, A.S., El-Shenawy, H.Z., El-Yazeed, W.A., 2013. Characterization of 12-molybdophosphoric acid supported on mesoporous silica MCM-41 and its catalytic performance in the synthesis of hydroquinone diacetate. *Appl. Surf. Sci.* 282, 217–225.
- Ahmed, S.A., Tanaka, M., Hi Ando, K., Tawa, K.K., 2004. *Tetrahedron* 60 (28), 6029–6036.
- Al-Shehri, B.M., Shkir, M., Khder, A.S., Kaushik, A., Hamdy, M.S., 2020. Noble metal nanoparticles incorporated siliceous TUD-1 mesoporous nano-catalyst for low-temperature oxidation of carbon monoxide. *Nanomaterials* 10, 1067–1079.
- Altass, H.M., Khder, A.E.R.S., 2016. Surface and catalytic properties of triflic acid supported zirconia: effect of zirconia tetragonal phase. *J. Mole. Catal. A Chem.* 411, 138–145.
- Altass, H.M., Khder, A.E.R.S., 2018. Catalytic oxidation of carbon monoxide over of gold-supported iron oxide catalyst. *Mater. Res. Innov.* 22, 107–114.
- Altass, H.M., Khder, A.E.R.S., 2018. Preparation, characterization of highly active recyclable zirconium and tin tungstate catalysts and their application in Pechmann condensation reaction. *React. Kinet. Mech. Catal.* 125, 227–243.
- Altass, H.M., Khder, A.S., Ahmed, S.A., Morad, M., Alsabei, A.A., Jassas, R.S., Althagafy, K., Ahmed, A.I., Salama, R.S., 2021. Highly efficient, recyclable cerium-phosphate solid acid catalysts for the synthesis of tetrahydrocarbazole derivatives by Borsche-Drechsel cyclization. *React. Kinet. Mech. Catal.* 134, 143–161.
- Arata, K., 1996. Preparation of superacids by metal oxides for reactions of butanes and pentanes. *Appl. Catal. A Gen.* 146, 3–32.
- Banares, M.A., Wachs, I.E., 2002. Molecular structures of supported metal oxide catalysts under different environments. *J. Raman Spectrosc.* 33 (5), 359–380.
- Bigey, C., Hilaire, L., Maire, G., 2001. WO_3 - CeO_2 and Pd/WO_3 - CeO_2 as potential catalysts for reforming applications: I. Physicochemical characterization study. *J. Catal.* 198, 208–222.
- Bilal, A.M., Rasool, N., Khan, S.G., Rashid, U., Altaf, H., Ali, I., 2021. Synthesis of indoles via intermolecular and intramolecular cyclization by using palladium-based catalysts. *Catalysts* 11 (9), 1018–1098.
- Cai, S., Lin, S., Yi, X., Xi, C., 2017. Substrate-controlled transformation of azobenzenes to indazoles and indoles via Rh(III)-catalysis. *J. Org. Chem.* 82 (1), 512–520.
- Caiuby, C.A.D., de Jesus, M.P., Burtoloso, A.C.B., 2020. α -Imino iridium carbenes from imidoyl sulfoxonium ylides: application in the one-step synthesis of indoles. *J. Org. Chem.* 85 (11), 7433–7445.
- Cao, W., Ju, P., Wang, Z., Zhang, Y., Zhai, X., Jiang, F., Sun, C., 2020. Colorimetric detection of H_2O_2 based on the enhanced peroxidase mimetic activity of nanoparticles decorated $Ce_2(WO_4)_3$ nanosheets. *Spectrochim. Acta A Mol. Biomol. Spectrosc.* 239, 118499–118508.
- Chung, H., Kim, J., González-Montiel, G.A., Cheong, P.H., Lee, H. G., 2021. Modular counter-Fischer–Indole synthesis through radical-enolate coupling. *Org. Lett.* 23 (3), 1096–1102.
- Cui, X., Qiao, X., Wang, H., Huang, G., 2020. Iridium (III)-catalyzed tandem annulation of pyridine-substituted anilines and α -Cl ketones for obtaining 2-arylindoles. *J. Org. Chem.* 85 (21), 13517–13528.
- Devkota, S., Kim, S., Yoo, S.Y., Mohandoss, S., Baik, M., Lee, Y.R., 2021. Ruthenium(II)-catalyzed regioselective direct C4- and C5-diamidation of indoles and mechanistic studies. *Chem. Sci.* 12 (34), 11427–11437.
- Dirany, N., Arab, M., Moreau, A., Valmalette, J.C., Gavarri, J.R., 2016. Hierarchical design and control of $NaCe(WO_4)_2$ crystals: structural and optical properties. *Cryst. Eng. Comm.* 18, 6579–6593.
- El-Hakam, S.A., El-Khouly, A.A., Khder, A.S., 1999. Surface properties and catalytic activity of Ni/Al_2O_3 - $AlPO_4$ catalysts. *Adsorp. Sci. Technol.* 17, 417–430.
- El-Hakam, S.A., El-Khouly, A.A., Khder, A.S., 1999. Effect of thermal treatment on various characteristics of nickel/aluminum phosphate catalysts. *Appl. Catal. A: Gen.* 185, 247–257.
- Farahmandjou, M., Zarinkamar, M., Firoozabadi, T.P., 2016. Synthesis of Cerium Oxide (CeO_2) nanoparticles using simple CO-precipitation method. *Rev. Mex. de Fis.* 62 (5), 496–499.
- Fischer, E., Jourdan, F., 1883. Ueber die hydrazine der brenztraubensäure. *Ber. Dtsch. Chem. Ges.* 16, 2241–2245.
- Fouad, O.A., Khder, A.E.R.S., Dai, Q., El-Shall, M.S., 2011. Structural and catalytic properties of ZnO and Al_2O_3 nanostructures loaded with metal Nanoparticles. *J. Nanopart. Res.* 13, 7075–7083.
- Geng, Y., Xiong, S., Li, B., Liao, Y., Xiao, X., Yang, S., 2018. $H_3PW_{12}O_{40}$ grafted on CeO_2 : a high-performance catalyst for the selective catalytic reduction of NO_x with NH_3 . *Ind. Eng. Chem. Res.* 57 (3), 856–866.
- Guo, R., Chen, J., 2018. Recent advances in the synthesis of fluorinated hydrazones. *RSC Adv.* 8 (31), 17110–17120.
- Guptaa, V.K., Pathania, D., Singh, P., Kumar, A., Rathore, B.S., 2014. Adsorption removal of methylene blue by guar gum–cerium (IV)tungstate hybrid cationic exchanger. *Carbohydr. Polym.* 101, 684–691.
- Hassan, H.M.A., Betiha, M.A., Khder, A.E.R.S., Mostafa, M., Gallab, M., 2016. Hafnium pentachloride ionic liquid for isomorphous and post synthesis of HfKIT-6 mesoporous silica: catalytic performances of $Pd/SO_4^{2-}/HfKIT-6$. *J. Porous Mater.* 23, 1339–1351.
- Ibrahim, A.A., Salama, R.S., El-Hakam, S.A., Khder, A.S., Ahmed, A.I., 2021. Synthesis of sulfated zirconium supported MCM-41 composite with high-rate adsorption of methylene blue and excellent heterogeneous catalyst. *Colloids Surf. A Physicochem. Eng. Asp.* 616, 126361–126372.
- Inomata, M., Kishida, K., Maruyama, Y., Watanabe, T., 2015. Synthesis of a new scheelite type Eu^{3+} doped $Gd_2W_2O_9$ red light emitting phosphor by the polymerized complex method. *Solid State Sci.* 48, 251–255.
- Jafarpour, F., Ghasemi, M., Navid, H., Safaie, N., Rajai-Daryasarei, S., Habibi, A., Ferrier Jr., R.C., 2020. Assembly of indole cores through a palladium-catalyzed metathesis of Ar–X σ -bonds. *Org. Lett.* 22 (24), 9556–9561.
- Khder, A.E.R.S., 2008. Preparation, characterization and catalytic activity of tin oxide-supported 12-tungstophosphoric acid as a solid catalyst. *Appl. Catal. A: Gen.* 343, 109–116.
- Khder, A.S., Ahmed, A.I., 2009. Selective nitration of phenol over nanosized tungsten oxide supported on sulfated SnO_2 as a solid acid catalyst. *Appl. Catal. A: Gen.* 354, 153–160.
- Khder, A.E.R.S., Hassan, H.M.A., El-Shall, M.S., 2012. Acid catalyzed organic transformations by heteropoly tungstophosphoric acid supported on MCM-41. *Appl. Catal. A Gen.* 411, 77–86.
- Khder, A.E.R.S., Hassan, H.M.A., Betiha, M.A., Khairou, K.S., Ibrahim, A.A., 2014. CO oxidation over Au and Pd nanoparticles supported on ceria–hafnia mixed oxides. *React. Kinet. Mechan. Catal.* 112, 61–75.

- Khder, A.E.R.S., Ashour, S.S., Altass, H.M., Khairou, K.S., 2016. Pd nanoparticles supported on iron oxide nanorods for CO oxidation: Effect of preparation method. *J. Environ. Chem. Eng.* 4, 4794–4800.
- Khder, A.E.R.S., Ahmed, S.A., Altass, H.M., 2016. Mesoporous metal (IV) phosphates as high-performance acid catalysts for the synthesis of photochromic bis-naphthopyran via Claisen rearrangement. *React. Kinet. Mech. Catal.* 117, 745–759.
- Khder, A.E.R.S., Ahmed, S.A., Khairou, K.S., Altass, H.M., 2018. Competent, selective and high yield of 7-hydroxy-4-methyl coumarin over sulfonated mesoporous silica as solid acid catalysts. *J. Porous Mater.* 25, 1–13.
- Khder, A.S., El-Sharkawy, E.A., El-Hakam, S.A., Ahmed, A.I., 2008. Surface characterization and catalytic activity of sulfated tin oxide catalyst. *Catal. Commun.* 9 (5), 769–777.
- Khder, A.S., Morad, M., Altass, H.M., Ibrahim, A.A., Ahmed, S.A., 2021. Unprecedented green chemistry approach: tungstophosphoric acid encapsulated in MOF 199 as competent acid catalyst for some significant organic transformations. *J. Porous Mater.* 28 (1), 129–142.
- Kishida, K., Watanabe, T., 2014. Photocatalytic properties of lanthanide tungstates $\text{Ln}_2\text{W}_2\text{O}_9$ (Ln = La, Pr, Nd, Sm, and Gd). *J. Phys. Chem. Solids* 75, 486–490.
- Kobayashi, M., Miyoshi, K., 2007. $\text{WO}_3\text{-TiO}_2$ monolithic catalysts for high temperature SCR of NO by NH_3 : Influence of preparation method on structural and physico-chemical properties, activity and durability. *Appl. Catal. B Environ.* 72, 253–261.
- Koschker, P., Breit, B., 2016. Branching out: rhodium-catalyzed allylation with alkynes and allenes. *Acc. Chem. Res.* 49 (8), 1524–1536.
- Kuba, S., Lukinskas, P., Ahmad, R., Jentoft, F.C., Grasselli, R.K., Gates, B.C., Knözinger, H., 2003. Reaction pathways in n-pentane conversion catalyzed by tungstated zirconia: effects of platinum in the catalyst and hydrogen in the feed. *J. Catal.* 219, 376–388.
- Kulkarni, R.M., Pradima, J.B., Archana, N., Syed, S., Deeksha, A., Bhagyalakshmi, C., 2020. Kinetic studies on the synthesis of fuel additives from glycerol using $\text{CeO}_2\text{-ZrO}_2$ metal oxide catalyst. *Biofuel Res. J.* 7 (1), 1100–1108.
- Kumar, J.V., Karthik, R., Chen, S.M., Balasubramanian, P., Muthuraj, V., Selvam, V., 2017. A novel cerium tungstate nanosheets modified electrode for the effective electrochemical detection of carcinogenic nitrite ions. *Electroanalysis* 29, 2385–2394.
- Lei, F., Bing, Y., 2011. Surfactant-assisted hydrothermal process, shape-control, and photoluminescence of Eu^{3+} -doped lutetium tungstate microspheres. *J. Mater. Res.* 26, 88–95.
- Li, X., Li, X., Zhu, T., Peng, Y., Li, J., Hao, J., 2018. Extraordinary deactivation offset effect of arsenic and calcium on $\text{CeO}_2\text{-WO}_3$ SCR catalysts. *Environ. Sci. Technol.* 52, 8578–8587.
- Liu, W., Feng, L., Zhang, C., Yang, H., Guo, J., Liu, X., Zhang, X., Yang, Y., 2013. A facile hydrothermal synthesis of 3D flowerlike CeO_2 via a cerium oxalate precursor. *J. Mater. Chem. A* 1 (23), 6942–6948.
- Liu, W., Lei, T., Song, Z., Yang, X., Wu, C., Jiang, X., Chen, B., Tung, C., Wu, L., 2017. Visible light promoted synthesis of indoles by single photosensitizer under aerobic conditions. *Org. Lett.* 19 (12), 3251–3254.
- Luo, M., Chen, J., Chen, L., Lu, J., Feng, Z., Li, C., 2001. Structure and redox properties of $\text{Ce}_x\text{Ti}_{1-x}\text{O}_2$ solid solution. *Chem. Mater.* 13, 197–202.
- Ma, N., Li, P., Wang, Z., Dai, Q., Hu, C., 2018. Synthesis of indoles from aroyloxycarbamates with alkynes via decarboxylation/cyclization. *Org. Biomol. Chem.* 16 (14), 2421–2426.
- Maensiri, S., Masingboon, C., Laokul, P., Jareonboon, W., Promarak, V., Anderson, P.L., Seraphin, S., 2007. Egg white synthesis and photoluminescence of platelike clusters of CeO_2 nanoparticles. *Cryst. Growth Des.* 7, 950–955.
- Mamede, A.S., Payen, E., Grange, P., Poncelet, G., Ion, A., Alifanti, M., Pârvulescu, V.I., 2004. Characterization of WO_3/CeO_2 catalysts and their reactivity in the isomerization of hexane. *J. Catal.* 223 (1), 1–12.
- Maurya, R.K., Patel, O.P.S., Anand, D., Yadav, P.P., 2018. Substrate selective synthesis of indole, tetrahydroquinoline and quinoline derivatives via intramolecular addition of hydrazones and imines. *Org. Chem. Front.* 5 (7), 1170–1175.
- Mkhwanazi, B.N., van Heerden, F.R., Mavondo, G.A., Mabandla, M. V., Musabayane, C.T., 2019. Triterpene derivative improves the renal function of streptozotocin-induced diabetic rats: a follow-up study on maslinic acid. *Ren. Fail.* 41, 547–554.
- Nazeri, M.T., Farhid, H., Mohammadian, R., Shaabani, A., 2020. Cyclic imines in ugi and ugi-type reactions. *ACS Comb. Sci.* 22 (8), 361–400.
- Parwaiz, S., Bhunia, K., Das, A.K., Khan, M.M., Pradhan, D., 2017. Cobalt-doped ceria/reduced graphene oxide nanocomposite as an efficient oxygen reduction reaction catalyst and supercapacitor material. *J. Phys. Chem. C* 121 (37), 20165–20176.
- Peng, Y., Li, K., Li, J., 2013. Identification of the active sites on $\text{CeO}_2\text{-WO}_3$ catalysts for SCR of NO_x with NH_3 : An in-situ IR and Raman spectroscopy study. *Appl. Catal. B: Environ.* 140–141, 483–492.
- Pramanik, S., Bhattacharya, S.C., 2010. Size tunable synthesis and characterization of cerium tungstate nanoparticles via H₂O/AOT/heptane microemulsion. *Mate. Chem. Phys.* 121, 125–130.
- Ross-Medgaarden, E.I., Wachs, I.E., 2007. Structural determination of bulk and surface tungsten oxides with UV-vis diffuse reflectance spectroscopy and Raman spectroscopy. *J. Phys. Chem. C* 111 (41), 15089–15099.
- Roy, M.S., Meng, X., Koda, K., Rasapalli, S., Gout, D., Lovely, C.J., 2019. Total synthesis of (–)-haploscleridamine. *Tetrahedron Lett.* 60, 979–982.
- Ruiz-Castillo, P., Buchwald, S.L., 2016. Applications of palladium-catalyzed C–N cross-coupling reactions. *Chem. Rev.* 116 (19), 12564–12649.
- Shan, W., Liu, F., He, H., Shia, X., Zhang, C., 2011. Novel cerium-tungsten mixed oxide catalyst for the selective catalytic reduction of NO_x with NH_3 . *Chem. Comm.* 47, 8046–8048.
- Shan, W., Liu, F., He, H., Shi, X., Zhang, C., 2012. A superior Ce–W–Ti mixed oxide catalyst for the selective catalytic reduction of NO_x with NH_3 . *Appl. Catal. B Environ.* 115–116, 100–106.
- Sing, K.S.W., Everett, D.H., Haul, R.A.W., Moscou, L., Pierotti, R. A., Rouqu rol, J., Siemieniowska, T., 1985. Reporting physisorption data for gas/solid systems with special reference to the determination of surface area and porosity. *Pure Appl. Chem.* 57, 603–619.
- Sugiura, K., Ogo, S., Iwasaki, K., Yabe, T., Sekine, Y., 2016. Low-temperature catalytic oxidative coupling of methane in an electric field over a Ce–WO catalyst system. *Sci. Rep.* 6 (1), 25154–25163.
- Thakur, S., Patil, P., 2014. Rapid synthesis of cerium oxide nanoparticles with superior humidity-sensing performance. *Sens. Actuators B Chem.* 194, 260–268.
- Tomasulo, M., Kaanumal, S.L., Sortino, S., Raymo, F.M., 2007. *J. Org. Chem.* 72, 595–605.
- Venkatesh, K.S., Gopinath, K., Palani, N.S., Arumugam, A., Jose, S. P., Bahadur, S.A., Ilangoan, R., 2016. Plant pathogenic fungus *F. solani* mediated biosynthesis of nanoceria: antibacterial and antibiofilm activity. *RSC adv.* 6 (48), 42720–42729.
- Yong Kim, T., Park, D.S., Choi, Y., Baek, J., Park, J.R., Yi, J., 2012. Preparation and characterization of mesoporous $\text{Zr-WO}_3/\text{SiO}_2$ catalysts for the esterification of 1-butanol with acetic acid. *J. Mater. Chem.* 22, 10021–10028.
- Yuzhakova, T., Rakić, V., Guimon, C., Auroux, A., 2007. Preparation and characterization of $\text{Me}_2\text{O}_3\text{-CeO}_2$ (Me = B, Al, Ga, In) mixed-oxide catalysts. *Chem. Mater.* 19 (12), 2970–2981.
- Zhou, Y., Song, Q., 2018. Oxidative ring-opening of 3-aminoindazoles for the synthesis of 2-aminobenzoates. *Org. Chem. Front.* 5, 3245–3249.